 https://doi.org/10.24191/jeesr.v29i1.018

Layer Dependent Raman and SERS Response of Gold Thin Film-Based Hybrid Substrate

Aida Zulia Zulhanip*, Nor Shahanim Mohamad Hadis, Anis Diyana Rosli, Nur Atiqah Azman, and Nor Fadzilah Mokhtar

***Abstract*— The layer-dependent Raman and Surface-Enhanced Raman Scattering (SERS) responses on a planar gold thin film-based hybrid substrate are systematically investigated using Rhodamine 6G (R6G, 1 x 10^{-4} M) as a Raman probe molecule. Four substrate configurations of one-, two- and three-layer based on gold thin film (GTF), graphene quantum dots (GQDs) and gold nanoparticles (AuNPs) were evaluated through Raman spectroscopy. A glass slide served as a supporting platform for a 50 nm gold thin film onto GQDs and AuNPs, which were sequentially introduced to construct GTF, GQDs/GTF, AuNPs/GTF and AuNPs/GQDs/GTF substrates. The objective of this study is intentionally designed as comparative structural benchmarking rather than as a sensitivity or detection limit comparison practice. Raman spectra were measured using a 785 nm excitation laser to allow direct comparison of enhancement behaviour. The bare GTF exhibits weak Raman activity, while moderate enhancement was observed for two-layer substrates. However, the three-layer substrate demonstrated the highest Raman enhancement across all characteristic R6G vibrational modes. The substantial enhancement is attributed to the synergistic interaction between the localized surface plasmon resonance (LSPR) of AuNPs and GQDs, which further facilitates effective molecule-substrate interactions. The finding highlights the importance of the layer-response relationship that reveals how each additional functional layer contributes incrementally to Raman enhancement on a planar gold platform.**

***Index Terms*—gold nanoparticles (AuNPs), gold thin film (GTF), graphene quantum dots (GQDs), hybrid substrates, surface-enhanced Raman scattering (SERS).**

I. INTRODUCTION

Surface-Enhanced Raman Scattering (SERS) has been recognized as a powerful spectroscopic technique for ultrasensitive chemical and biological analysis due to its ability to amplify intrinsically weak Raman signals through electromagnetic (EM) and chemical (CE) enhancement mechanisms [1], [2]. In conventional SERS systems, EM is dominant and arises from localized surface plasmon resonance (LSPR) excitation in noble metal nanostructures especially gold and silver which generate intense near-field hotspots at nanogaps and distinct features [3]. Despite their high enhancement capability, colloidal metal nanoparticles SERS substrates often suffer from poor signal reproducibility and structural nonuniformity due to uncontrollable aggregation and random hotspot distribution [4]. These limitations remain a significant barrier to reliable quantitative sensing and large area implementation.

A solid SERS substrate comprising a planar gold thin film (GTF) on solid supports provides an impressive alternative due to its mechanical robustness, chemical stability and excellent signal uniformity across macroscopic areas overcoming the instability of colloidal systems [5]. However, the intrinsic Raman enhancement on flat metal films is typically weak due to the absence of strong plasmonic confinement [6], [7]. Various hybrid strategies have been proposed to overcome this limitation including surface roughening and three-dimensional nanoarchitectures [6], nanoparticles patterning [8] and integration with functional interlayers [9], [10] that can regulate molecule-analyte-surface interactions. In this context, the functional interlayer carbon nanomaterials has attracted increased attention due to its distinctive properties.

Carbon nanomaterials such as graphene, carbon nanotubes (CNTs), graphene oxide (GO) and graphene quantum dots (GQDs) exhibit remarkable properties including high electrical and thermal conductivity, large surface area, good mechanical strength and unique optical properties. Thanks to these features, graphene and its derivatives have been investigated in SERS-related studies in addition to their ability to enhance CE via charge-transfer mechanisms [11].

Zhang N. et al. (2025) demonstrate that graphene and its derivatives can produce graphene-based surface-enhanced Raman scattering (GERS) in which the enhancement factor arises predominantly from a CE mechanism via charge transfer between graphene and the absorbed molecules [12]. In the context of optical sensors, carbon-based nanomaterials have demonstrated high sensitivity and the ability to interact with a wide range of molecules via π–π stacking and charge transfer processes revealing their importance in metal-graphene hybrid SERS substrates [11]. In recent years, GQDs nanoscale fragments of graphene have emerged as a promising alternative to extended graphene sheets owing to their abundant edge defects, tunable band structures that control energy levels and abundant surface functional groups for chemical attachment [13], [14], [15]. These properties are assembled into GQDs to

This manuscript is submitted on January 28, 2026, revised on May 26, 2026, accepted on June 4, 2026 and published on October 31, 2026.

Aida Zulia Zulhanip, Nor Shahanim Mohamad Hadis, Anis Diyana Rosli, Nur Atiqah Azman and Nor Fadzilah Mokhtar are with Electrical Engineering Studies, Universiti Teknologi MARA Cawangan Pulau Pinang, Permatang Pauh Campus, Pulau Pinang, Malaysia.

*Corresponding author
Email address: aidazulia83@uitm.edu.my

1985-5389/© 2026 The Authors. Published by UiTM Press. This is an open access article under the CC BY-NC-ND license (http://creativecommons.org/licenses/by-nc-nd/4.0/).

effectively support molecular adsorption and interfacial electronic coupling when combined with plasmonic metals. Several studies have reported enhanced Raman or SERS responses in hybrid GQDs metal systems attributed to synergistic EM–CM enhancement effects [16], [17], [18].

Ramlan M. N. et al. (2025) demonstrate that silver (Ag) nanoparticles integrate with GQDs on a flexible fibreglass substrate. This integration reports significantly enhances SERS sensitivity toward dye molecules such as malachite green and methylene blue. The enhanced performance is associated with the cooperative EM–CE mechanism involving strong local fields from Ag nanoparticles and charge transfer interactions mediated by GQDs [17]. Another study reveals that the gold (Au)–NGQDs hybrid demonstrates much stronger SERS signals than bare Au nanoparticles in solutions. The Au cores generate intense EM hotspots while NGQDs wrapped around them modulate molecular adsorption and facilitate charge transfer, thereby enhancing synergistic EM–CE effects in the hybrid system [18].

However, many existing SERS studies focus primarily on target performance optimization or on detection limits involving specific analytes and multiple coupled parameters, such as nanoparticle size and shape, analyte concentration, surface area and substrate morphology [19], [20], [21]. Consequently, the individual contribution of each functional layer to the Raman response is rarely discussed. Besides, the incremental effect of introducing GQDs as an intermediate layer on planar GTF, followed by the addition of a plasmonic nanoparticle layer remains insufficiently explained. In this work, the gap was addressed by demonstrating a controlled layer-by-layer comparison of Raman responses resulting from one-layer GTF, two-layer GQDs/GTF, two-layer AuNPs/GTF and three-layer AuNPs/GQDs/GTF SERS substrates. R6G at a concentration of 1 x 10^{-4} is employed as a Raman probe molecule to provide clearly distinguishable SERS features, minimize concentration induced variability and emphasize the substrate-dependent effects [22].

Intentionally limiting this study to one representative three-layer configuration provides a simplified yet mechanistically informative assessment of how sequential layer assembly governs Raman enhancement on planar gold platforms. This understanding provides a structural basis for subsequent studies targeting low concentrations and application to specific sensing systems.

II. Materials and Methods

A. Substrate Fabrication and Layer-by-Layer Assembly

The layer-by-layer substrate configuration investigated in this work is shown systematically in Fig. 1. A planar GTF serves as a base layer, as shown in Fig. 1(a), followed by the deposition of GQDs to form a two-layer GQDs/GTF structure as shown in Fig. 1(b). The GQDs interlayer was deposited by drop-casting and allowed to dry under gentle heat treatment. For the alternative two-layer configuration, AuNPs were directly drop-cast onto the GTF to form the AuNPs/GTF substrate as in Fig. 1(c).

A single layer of AuNPs is subsequently initiated to obtain the three-layer AuNPs/GQDs/GTF substrate configuration as illustrated in Fig. 1(d). This schematic illustration clarifies the sequential assembly concept and the relative layer arrangement. A glass slide was included as a supporting platform for the 50 nm GTF to ensure mechanical stability.

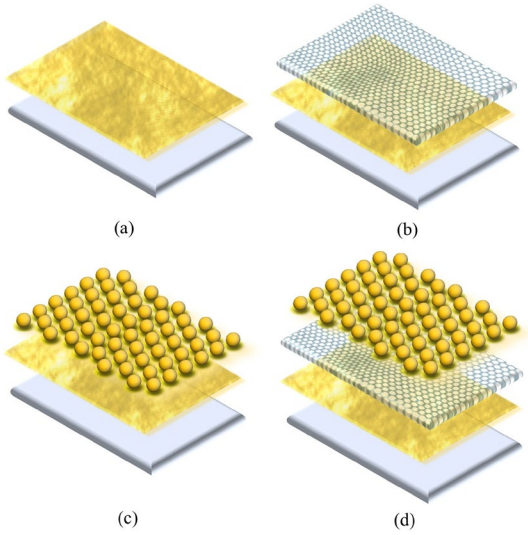


Fig. 1. Schematic illustration of the substrate architectures of (a) one-layer GTF, (b) two-layer GQDs/GTF, (c) two-layer AuNPs/GTF and (d) three-layer AuNPs/GQDs/GTF SERS substrates. The glass slide serves as a supporting platform for all configurations and is not considered a functional layer. The schematic is intended to illustrate the relative layer arrangement rather than thickness or scale.

B. Gold Thin Film (GTF)

GTF with a nominal thickness of 50 nm (±5 nm) were deposited on glass slides with a 5 nm chromium adhesion layer as a supporting platform for substrate fabrication and were commercially available and purchased directly from Ted Pella, Inc. The gold film has a purity of 99.99% and serves as the base plasmonic layer ensuring thickness, uniformity and reproducibility across all samples without further modification.

C. Gold Nanoparticles (AuNPs)

AuNPs were prepared using the citrate reduction (Turkevich) method following the standard chemical reduction procedures reported in [23]. Chloroauric acid ($HAuCl_4$) solution was prepared and heated under constant stirring. Trisodium citrate ($Na_3C_6H_5O_7$) was injected into the desired heated $HAuCl_4$ solution inducing the reduction of Au^{3+} ions and the formation of AuNPs, as indicated by a colour change from light yellow to ruby red upon cooling to room temperature. The ruby red AuNPs were obtained by a heating at 95°C while stirring at 1000 rpm with a magnetic stirrer. The final AuNPs solution yielded a stable colloidal AuNPs suspension without further modification as shown in Fig. 2(a).

D. Graphene Quantum Dots (GQDs)

GQDs were synthesized via a hydrothermal method using GO as a precursor following a previously reported method with some modifications [24]. Briefly, a predetermined GO powder was dispersed in NaOH solution and subjected to a hydrothermal treatment process at 200°C for 24 hours resulting in the oxidative cutting of graphene sheets into nanoscale GQDs. After naturally cooling to room temperature, the solution was purified to remove residual reactants from the hydrothermal treatment using centrifugation, filtration and dialysis yielding a final transparent GQDs solution as observed in Fig. 2(b).



(a) (b)

Fig. 2. Final solution of (a) synthesized ruby red AuNPs solution, (b) transparent GQDs solution via dialysis process.

E. Substrate Characterization and Raman Measurements

The optical absorption properties were characterized using a Shimadzu UV-Vis Spectroscopy/UV-1900i over a scanning range of 200-800 nm. The surface morphology, particle size distribution and coverage of the AuNPs were examined using a JEOL JSM-7600F Field Emission Scanning Electron Microscope (FESEM) operating at an accelerating voltage of 3.5 kV with a working distance (WD) of 4.3 mm. Raman spectra were collected using a PeekSeeker Raman Spectroscopy system (Agiltron PKR-785) equipped with a 785 nm excitation laser. The laser power was set to 100 mW to minimize laser-induced heating while maintaining sufficient signal intensity. Spectral acquisition involved signal accumulation across multiple scans to improve signal-to-noise ratio with consistent acquisition parameters applied to all measurement samples to ensure reliability. Raman spectra were recorded in the range of 550 – 1800 cm^{-1}. 10 randomly selected spots were measured across the functional area to evaluate substrate uniformity and signal reproducibility.

III. Results and Discussion

A. Structural and Optical Characterization of the Substrate

UV-Vis spectroscopy was conducted to evaluate the optical absorption characteristics of the fabricated AuNPs/GQDs/GTF substrate. As depicted in Fig. 3, distinct absorption bands were observed at ~290 nm and ~340 nm. The peak at ~ 290 nm is attributed to the π-π* transition of aromatic C=C bonds [25], [26], while the shoulder at ~340 nm corresponds to the n-π* transition associated with oxygen-containing functional groups of GQDs [26]. Furthermore, a broad absorption peak centered at ~538 nm corresponds to the characteristic LSPR of the integrated AuNPs [27], [28]. The existence of both absorption features indicates the successful integration of GQDs and AuNPs within the substrate structure.

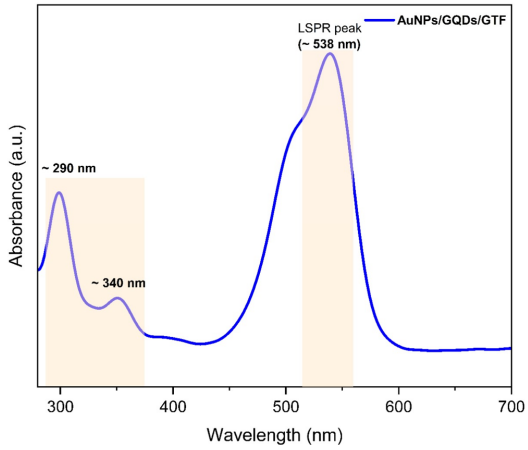
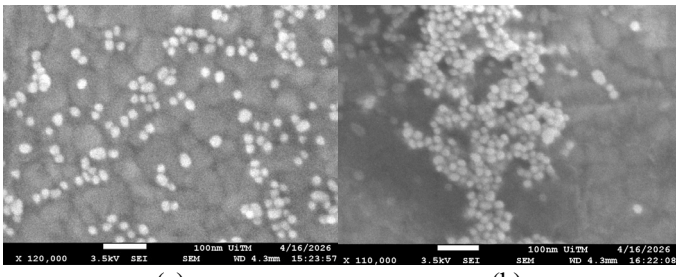


Fig. 3. UV-Vis absorption spectrum of the three-layer AuNPs/GQDs/GTF substrate.

Surface morphology including nanoparticle distribution and structural coverage was further anayzed using FESEM as shown in Fig. 4 which compares the structural distribution of the top plasmonic layer across two configurations. Fig. 4(a) demonstrates a two-layer AuNPs/GTF substrate in which the spherical AuNPs are uniformly distributed across the planar GTF. The nanoparticles demonstrate a consistent size distribution with minimal aggregation revealing the distinct interparticulate boundaries.

In contrast, Fig. 4(b) highlights the morphological surface of three-layer AuNPs/GQDs/GTF substrate. The introduction of the GQDs intermediate layer modifies the assembly behaviour yielded a significantly denser surface coverage of AuNPs. The high-density arrangement facilitates the configurations of closely spaced nanogaps across the platform. These structures are laying the exact foundation for high-density SERS hotspots [29], [30].



(a) (b)

Fig. 4. FESEM of AuNPs distributed on (a) the two-layer AuNPs/GTF substrate of x120000 magnification and, (b) the three-layer AuNPs/GQDs/GTF substrate of x110000 magnification.

B. Raman spectra of layer-dependent enhancement

Fig. 5 presents the Raman spectra analysis of a probe molecule, R6G at a concentration of 1 x 10^{-4} M obtained from four different substrate configurations under similar

experimental conditions. The comparison reveals that a single GTF layer and a combined GTF, GQDs/AuNPs material govern Raman enhancement behaviour.

Smooth metal films, referred to as pristine GTF exhibit negligible Raman features indicating their suitability as an inert reference surface as shown in Fig. 5(a). GTF shows weak signals consistent with the low Raman activity of smooth and flat thin metallic films [6], [7] due to the lack of nanoscale electromagnetic hotspots that require strong localized field confinement [7]. GTF thus serves as a reliable baseline reference for evaluating subsequent layer modifications.

Once GQDs are deposited onto the GTF substrate known as two-layer GQDs/GTF, weak Raman signals corresponding to R6G vibrational modes are observed as shown in Fig. 5(b). However, the two-layer GQDs/GTF signal intensity remains much lower than the plasmonic substrates of two-layer AuNPs/GTF as shown in Fig. 5(c). This shows that the GQDs alone cannot generate EM, as they do not support LSPR. The weak signals from two-layer GQDs/GTF are due to enhanced molecular adsorption and CE mechanisms facilitated by the oxygen-containing functional groups in GQDs [31]. These groups promote π–π interactions and electrostatic attraction between R6G molecules and the GQDs surface. This increases the effective Raman scattering cross-section but results only in modest CE rather than strong electromagnetic SERS.

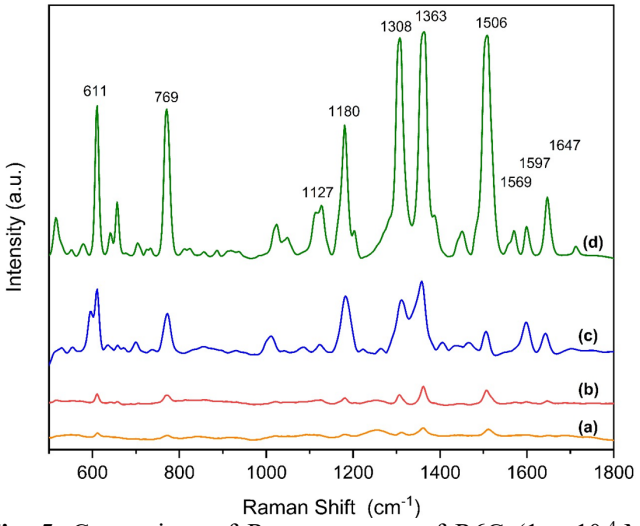


Fig. 5. Comparison of Raman spectra of R6G (1 x 10^{-4} M) obtained from (a) GTF, (b) GQDs/GTF, (c) AuNPs/GTF and (d) AuNPs/GQDs/GTF substrates under identical measurement conditions illustrating the layer-dependent enhancement of Raman intensity.

Conversely, the two-layer AuNPs/GTF reveals a well-defined and distinguishable Raman peak of R6G at approximately 611, 769, 1127, 1180, 1308, 1363, 1506, 1569, 1597 and 1647 cm^{-1} [25], [26]. The sharp peaks confirm the presence of plasmon-induced EM arising from LSPR of AuNPs. Numerous studies have established AuNPs as effective SERS substrates due to their ability to concentrate EM fields at nanoparticles and at metal-dielectric interfaces [27], [28]. However, the enhancement of the two-layer AuNPs/GTF remains moderate potentially due to limitations in nanoparticles distribution, interparticle spacing and coupling efficiency on the planar gold thin film surface.

Among the substrates, the three-layer AuNPs/GQDs/GTF SERS substrate showed the highest increase in Raman intensity for all major R6G vibrational modes as demonstrated in Fig. 5(d). It outperformed both two-layer configurations. The significant enhancements indicated a synergistic effect from the combined plasmonic and interfacial contributions of AuNPs and GQDs. In this architecture, AuNPs serve as the primary EM, while the GQDs interlayer plays a critical role in modulating molecule-substrate interactions and plasmonic coupling.

The characteristics of the observed Raman peaks of R6G which aid in understanding of molecular interactions and surface effects are summarized in Table I along with their significance in SERS analysis. The low-frequency mode at ~611 cm^{-1} is sensitive to EM and reflects hotspot efficiency. In contrast, the out-of-plane C-H bending mode at ~769 cm^{-1} provides information on molecular orientation and adsorption geometry. Molecule-surface interactions and local chemical environments are correlated with the ~1127 and ~1180 cm^{-1} bands.

The C-C stretching modes at ~1308 and ~1363 cm^{-1} correspond to conjugated ring vibrations with the latter serving as a stable reference peak for relative SERS intensity comparisons. EM and interfacial electronic interactions predominantly influenced high-frequency modes between ~1506 and ~1647 cm^{-1}. These assigned modes provide a basis for interpreting the layer-dependent Raman enhancement behaviour observed in the hybrid substrates.

TABLE I. CHARACTERISTICS OF RAMAN PEAKS FROM R6G COMPARISON ACROSS SUBSTRATE CONFIGURATION [29]

Peak	Vibrational Mode Assignment	Significance in SERS Analysis
~611	in-plane C-C-C ring bending	Sensitive to EM enhancement which is commonly used as a hotspot efficiency probe
~769	Out-of-plane C-H bending	Reflects molecular orientation and adsorption geometry on the substrate surface
~1127	C-H in-plane bending	Sensitive to molecule–surface interaction and local chemical environment
~1180	C-H in-plane bending (xanthene ring)	Associated with adsorption-induced interfacial interactions
~1308	aromatic C-C stretching	Moderately sensitive to charge-transfer related effects
~1363	aromatic C-C stretching	Strong and stable reference peak for relative SERS intensity comparison
~1506	C=C stretching	Dominant EM-enhanced modes which are commonly used to assess SERS activity
~1569	C-C stretching (ring mode)	Sensitive to electronic coupling between molecules and the substrate
~1597	C-C stretching (aromatic ring)	Sensitive to combining EM and interfacial interaction effects
~1647	C=C stretching (xanthene ring)	High-frequency mode sensitive to interfacial electronic interactions

GQDs between AuNPs and GTF enhance SERS performance through three mechanisms: 1) GQDs improve the adsorption

efficiency of R6G molecules by increasing the local analyte concentration near plasmonic hotspots, 2) the GQDs layer acts as a nanoscale spacer which optimizes the distance between AuNPs and the planar GTF to enhance the electromagnetic field coupling. Similar interlayer-mediated enhancements with graphene-based materials have been reported amplifying charge transfer and plasmonic interaction of Raman signals [30], [31]. Finally, 3) synergistic interaction between AuNPs-induced LSPR and GQDs-associated CE contributes to the main amplification of Raman scattering.

C. Statistical Validation and Reproducibility Analysis

To address the requirements for SERS signal uniformity, a multi-spot reproducibility analysis was performed on the AuNPs/GQDs/GTF substrate. Fig. 6 displays the overlay of SERS spectra collected from 10 randomly selected spots across the sample surface. The spectral profiles show good consistency with all main characteristic peaks of R6G maintained at stable positions and shapes across all measurements.

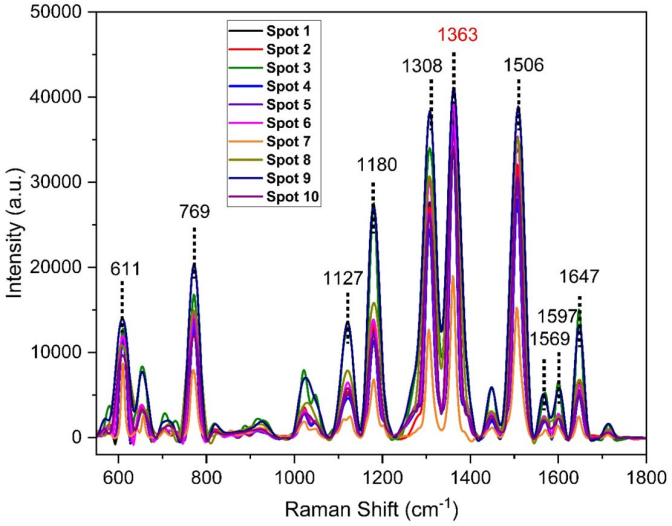


Fig.6. SERS spectra overlay of R6G (1 x 10^{-4} M) across the AuNPs/GQDs/GTF substrate under identical 785 nm laser excitation.

A quantitative statistical analysis was performed on the prominent C-C stretching mode at a 1363 cm^{-1} which is used as a reference peak for SERS intensity comparisons. The RSD value of 17.74% is an acceptable signal uniformity and reproducibility is considered acceptance for the drop-cast method used in the hybrid structure, as demonstrated in Fig. 7. This indicates that the layered configuration helps reduce the signal variations commonly found in non-uniform colloidal SERS systems.

Overall, the results demonstrate that while AuNPs are the dominant SERS-active component, integrating GQDs as an interfacial layer significantly enhances Raman performance by providing synergistic plasmonic-chemical enhancement mechanisms. Precisely, GQDs cannot function as independent SERS substrates but rather as an practical interlayers that amplify the plasmonic response of AuNPs when integrated into a layered architecture.

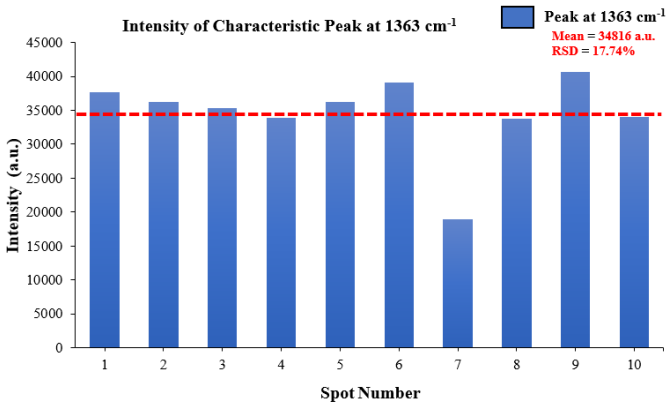


Fig. 7. Reproducibility and uniformity analysis of the SERS intensity variation at peak 1363 cm^{-1}.

IV. Conclusion

This work reports a direct comparison of Raman and SERS responses from one-, two- and three-layer planar substrates based on a GTF. The structural and optical integrity of the hybrid configurations was verified via FESEM and UV-Vis characterization. The one-layer GTF exhibits minimal Raman activity, whereas the addition of GQDs as a second layer activates carbon-related vibrational features and enhances R6G interaction. The addition of an AuNPs layer as the third layer results in precise, highly uniform (RSD=17.74%) and reproducible Raman intensity enhancement confirming the dominant role of plasmonic coupling at the AuNPs–GQDs–GTF interface. By intentionally limiting the work to a single representative three-layer configuration, this study provides a layer-by-layer assessment without overanalyzing. The finding serves as a concise structural reference for subsequent studies on optimized architecture and low concentration sensing.

Acknowledgment

The authors would like to acknowledge the Ministry of Higher Education (MOHE) for funding under the Fundamental Research Grant Scheme (FRGS/1/2023/TK07/UITM/02/26). Additionally, Universiti Teknologi MARA (UiTM) cawangan Shah Alam and UiTM cawangan Pulau Pinang for providing research facilities and technical support throughout this study.

References

[1] X. X. Han, R. S. Rodriguez, C. L. Haynes, Y. Ozaki, and B. Zhao, "Surface-enhanced Raman spectroscopy," *Nature Reviews Methods Primers*, vol. 1, no. 1, p. 87, Dec. 2021, doi: 10.1038/s43586-021-00083-6.

[2] V. Shvalya, G. Filipič, J. Zavašnik, I. Abdulhalim, and U. Cvelbar, "Surface-enhanced Raman spectroscopy for chemical and biological sensing using nanoplasmonics: The relevance of interparticle spacing and surface morphology," *Appl. Phys. Rev.*, vol. 7, no. 3, Sep. 2020, doi: 10.1063/5.0015246.

[3] M. K. Hossain, "Detection of surface enhanced Raman scattering active hotspot using near field scanning optical microscopy," *Sci. Rep.*, vol. 14, no. 1, p. 10559, Dec. 2024, doi: 10.1038/s41598-024-61503-7.

[4] S. Sloan-Dennison, G. Q. Wallace, W. A. Hassanain, S. Laing, K. Faulds, and D. Graham, "Advancing SERS as a quantitative technique: challenges, considerations, and correlative approaches to aid validation," *Nano Converg.*, vol. 11, no. 1, p. 33, Dec. 2024, doi: 10.1186/s40580-024-00443-4.

[5] K. Ge, Y. Hu, and G. Li, "Recent Progress on Solid Substrates for Surface-Enhanced Raman Spectroscopy Analysis," *Biosensors (Basel).*, vol. 12, no. 11, p. 941, Nov. 2022, doi: 10.3390/bios12110941.

[6] X. Zhou *et al.*, "Three-dimensional SERS substrates: Architectures, hot spot engineering, and biosensing applications," *Biosensors (Basel).*, vol. 15, no. 9, p. 555, Sep. 2025, doi: 10.3390/bios15090555.

[7] C. Lee, C. S. Robertson, A. H. Nguyen, M. Kahraman, and S. Wachsmann-Hogiu, "Thickness of a metallic film, in addition to its roughness, plays a significant role in SERS activity," *Sci. Rep.*, vol. 5, no. 1, p. 11644, Jun. 2015, doi: 10.1038/srep11644.

[8] O. Geladari *et al.*, "Direct laser induced writing of high precision gold nanosphere SERS patterns," *Nanoscale Adv.*, vol. 6, no. 4, pp. 1213–1217, Feb. 2024, doi: 10.1039/d3na00855j.

[9] Y. Xu, Y. Zhang, C. Li, Z. Ye, and S. E. J. Bell, "SERS as a Probe of Surface Chemistry Enabled by Surface-Accessible Plasmonic Nanomaterials," *Acc. Chem. Res.*, vol. 56, no. 15, pp. 2072–2083, Aug. 2023, doi: 10.1021/acs.accounts.3c00207.

[10] C. Deriu and L. Fabris, "A surface chemistry perspective on SERS: revisiting the basics to push the field forward," *Chem. Soc. Rev.*, vol. 54, no. 11, pp. 5224–5247, Mar. 2025, doi: 10.1039/d4cs01242a.

[11] X. G. Gao, L. X. Cheng, W. S. Jiang, X. K. Li, and F. Xing, "Graphene and its Derivatives-Based Optical Sensors," *Front. Chem.*, vol. 9, p. 615164, Feb. 2021, doi: 10.3389/fchem.2021.615164.

[12] N. Zhang, L. Tong, and J. Zhang, "Graphene-based enhanced Raman scattering toward analytical applications," *Chemistry of Materials*, vol. 28, no. 18, pp. 6426–6435, Sep. 2016, doi: 10.1021/acs.chemmater.6b02925.

[13] A. Sheely, B. Gifford, S. Tretiak, and A. Bishop, "Tunable Optical Features of Graphene Quantum Dots from Edge Functionalization," *Journal of Physical Chemistry C*, vol. 125, no. 17, pp. 9244–9252, May 2021, doi: 10.1021/acs.jpcc.1c00537.

[14] P. Kadyan *et al.*, "Comprehensive Review on Synthesis, Applications, and Challenges of Graphene Quantum Dots (GQDs)," *J. Nanomater.*, vol. 2023, no. 1, p. 2832964, 2023, doi: 10.1155/2023/2832964.

[15] R. Rabeya, S. Mahalingam, A. Manap, M. Satgunam, M. Akhtaruzzaman, and C. H. Chia, "Structural defects in graphene quantum dots: A review," *Int. J. Quantum Chem.*, vol. 122, no. 12, p. e26900, Jun. 2022, doi: 10.1002/qua.26900.

[16] R. Mandavkar *et al.*, "Hybrid SERS platform by adapting both chemical mechanism and electromagnetic mechanism enhancements: SERS of 4-ATP and CV by the mixture with GQDs on hybrid PdAg NPs," *Surfaces and Interfaces*, vol. 33, p. 102175, Oct. 2022, doi: 10.1016/j.surfin.2022.102175.

[17] N. M. Ramlan, I. Isnaeni, A. F. Afiff, M. M. Suliyanti, and D. Tahir, "Development of flexible SERS substrates based on silver nanoparticles and graphene quantum dots on fiberglass for enhanced dye detection," *Environ. Nanotechnol. Monit. Manag.*, p. 101094, Dec. 2025, doi: 10.1016/j.enmm.2025.101094.

[18] X. Miao *et al.*, "Graphene Quantum Dots Wrapped Gold Nanoparticles with Integrated Enhancement Mechanisms as Sensitive and Homogeneous Substrates for Surface-Enhanced Raman Spectroscopy," *Anal. Chem.*, vol. 91, no. 11, pp. 7295–7303, Jun. 2019, doi: 10.1021/acs.analchem.9b01001.

[19] V. Dzhagan *et al.*, "Self-Organized SERS Substrates with Efficient Analyte Enrichment in the Hot Spots," *ACS Omega*, vol. 9, no. 4, pp. 4819–4830, Jan. 2024, doi: 10.1021/acsomega.3c08393.

[20] S. Kenmotsu *et al.*, "Surface-Enhanced Raman Scattering on Size-Classified Silver Nanoparticles Generated by Laser Ablation," *ACS Omega*, vol. 9, no. 36, pp. 37716–37723, Sep. 2024, doi: 10.1021/acsomega.4c03046.

[21] F. Scaglione, L. Battezzati, and P. Rizzi, "Breaking Down SERS Detection Limit: Engineering of a Nanoporous Platform for High Sensing and Technology," *Nanomaterials*, vol. 12, no. 10, p. 1737, May 2022, doi: 10.3390/nano12101737.

[22] K. O. Ay, "DETECTION OF RHODAMINE VIA SURFACE ENHANCED RAMAN SPECTROSCOPY UTILISING AG NANOWIRES," *Eskişehir Technical University Journal of Science and Technology A - Applied Sciences and Engineering*, vol. 24, no. 4, pp. 240–249, Dec. 2023, doi: 10.18038/estubtda.1237440.

[23] J. Dong, P. L. Carpinone, G. Pyrgiotakis, P. Demokritou, and B. M. Moudgil, "Synthesis of precision gold nanoparticles using Turkevich method," *KONA Powder and Particle Journal*, vol. 37, pp. 224–232, 2020, doi: 10.14356/kona.2020011.

[24] D. Mukherjee, P. Das, S. Kundu, and B. Mandal, "Engineering of graphene quantum dots by varying the properties of graphene oxide for fluorescence detection of picric acid," *Chemosphere*, vol. 300, p. 134432, Aug. 2022, doi: 10.1016/j.chemosphere.2022.134432.

[25] T. E. Timofeeva, M. N. Egorova, and A. E. Tomskaya, "Calculations of electronic absorption spectra of polyciclic aromatic hydrocarbon models of graphene quantum dots," in *AIP Conference Proceedings*, American Institute of Physics Inc., Mar. 2021. doi: 10.1063/5.0042367.

[26] S. Dorontić, S. Jovanović, and A. Bonasera, "Shedding light on graphene quantum dots: Key synthetic strategies, characterization tools, and cutting-edge applications," *Materials*, vol. 14, no. 20, Oct. 2021, doi: 10.3390/ma14206153.

[27] S. Wadhwa *et al.*, "Engineering of luminescent graphene quantum dot-gold (GQD-Au) hybrid nanoparticles for functional applications," *MethodsX*, vol. 7, Jan. 2020, doi: 10.1016/j.mex.2020.100963.

[28] J. A. Jenkins *et al.*, "Blue-Shifted Narrow Localized Surface Plasmon Resonance from Dipole Coupling in Gold Nanoparticle Random Arrays," *Journal of Physical Chemistry C*, vol. 118, no. 45, pp. 26276–26283, Nov. 2014, doi: 10.1021/jp508181g.

[29] C. Zhang *et al.*, "SERS activated platform with three-dimensional hot spots and tunable nanometer gap," *Sens. Actuators B Chem.*, vol. 258, pp. 163–171, Apr. 2018, doi: 10.1016/j.snb.2017.11.080.

[30] X. Meng, L. Qiu, G. Xi, X. Wang, and L. Guo, "Smart design of high-performance surface-enhanced Raman scattering substrates," *SmartMat*, vol. 2, no. 4, pp. 466–487, Dec. 2021, doi: 10.1002/smm2.1058.

[31] J. Ge, Y. Li, J. Wang, Y. Pu, W. Xue, and X. Liu, "Green synthesis of graphene quantum dots and silver nanoparticles compounds with excellent surface enhanced Raman scattering performance," *J. Alloys Compd.*, vol. 663, pp. 166–171, Apr. 2016, doi: 10.1016/j.jallcom.2015.12.055.

[32] F. Zhong, Z. Wu, J. Guo, and D. Jia, "Porous silicon photonic crystals coated with Ag nanoparticles as efficient substrates for detecting trace explosives using SERS," *Nanomaterials*, vol. 8, no. 11, p. 872, Nov. 2018, doi: 10.3390/nano8110872.

[33] H. N. Khan *et al.*, "Enhanced SERS performance of gold nanoparticle assemblies on a cysteine-mutant Tobacco mosaic virus scaffold," *Journal of Science: Advanced Materials and Devices*, vol. 9, no. 4, p. 100775, Dec. 2024, doi: 10.1016/j.jsamd.2024.100775.

[34] A. Arbuz, A. Sultangaziyev, A. Rapikov, Z. Kunushpayeva, and R. Bukasov, "How gap distance between gold nanoparticles in dimers and trimers on metallic and non-metallic SERS substrates can impact signal enhancement," *Nanoscale Adv.*, vol. 4, no. 1, pp. 268–280, Jan. 2022, doi: 10.1039/d1na00114k.

[35] V. Cucuiet, D. Maniu, S. Astilean, M. Lamy de la Chapelle, and M. Focsan, "Graphene-mediated surface enhanced Raman spectroscopy for DNA Detection&hybridization: Breakthroughs and challenges," *Biosens. Bioelectron.*, vol. 286, p. 117610, Oct. 2025, doi: 10.1016/j.bios.2025.117610.

[36] Y. Zhao, S. Zhao, L. Zhang, Y. Liu, X. Li, and Y. Lu, "A three-dimensional Au nanoparticle-monolayer graphene-Ag hexagon nanoarray structure for high-performance surface-enhanced Raman scattering," *RSC Adv.*, vol. 7, no. 20, pp. 11904–11912, 2017, doi: 10.1039/c6ra27973b.